

# Subsonic and Supersonic Jet Noise Predictions from Statistical Source Models

Christophe Bailly\*

*École Centrale de Lyon, Ecully cedex 69131, France*

Philippe Lafon†

*Électricité de France, Clamart cedex 92141, France*

and

Sébastien Candel‡

*École Centrale Paris, Châtenay-Malabry cedex 92295, France*

Subsonic and supersonic jet noise is determined numerically from statistical source models. The goal is to develop prediction methods for high-speed jet noise for application to aeronautical and space transportation systems. In this framework, a combination of a  $k$ - $\epsilon$  turbulence closure with an acoustic analogy provides an interesting way to compute such radiated acoustic fields. Three acoustic analogies are investigated. First, the classical Lighthill theory in combination with Ribner's results is applied to calculate jet mixing noise. The second method relies on the Goldstein-Howes convected wave equation, which is used to improve the predicted supersonic jet mixing noise in the upstream direction. It is necessary to properly account for acoustic wave convection, and then, one finds that the Doppler factor features an exponent of  $-3$  in the associated power law. A model based on the Ffowcs Williams-Maidanik analysis then is developed to estimate the Mach-wave noise component that dominates forward arc radiation when the convection Mach number is supersonic. Comparisons between aerodynamic and calculated acoustic results on the one hand, and available measurements on the other hand, are carried out. It is shown that the last two models yield improved supersonic jet mixing noise predictions.

## Nomenclature

$C$  = Doppler or convection factor  
 $c$  = speed of sound  
 $D$  = exit nozzle diameter  
 $D_\theta$  = directivity of shear noise  
 $k$  = turbulent kinetic energy  
 $L$  = turbulence integral longitudinal length scale  
 $M$  = jet exit Mach number,  $M = U_j/c_j$   
 $M_c$  = convection Mach number,  $M_c = U_c/c_o$   
 $p$  = pressure  
 $R_a$  = pressure autocorrelation function; the Fourier transform of  $R_a$  is defined by  
 $S_a(\mathbf{x}, \omega) = (1/2\pi) \int R_a(\mathbf{x}, \tau) \exp(i\omega\tau) d\tau$   
 $S_a$  = power spectral density  
 $\mathbf{U}$  = mean flow velocity  
 $U_c$  = convection velocity of turbulent eddies  
 $U_j$  = jet exit velocity  
 $\mathbf{u}$  = velocity  
 $u'$  = turbulence velocity scale,  $u' = 2k/3$   
 $\mathbf{x}$  = observer position  
 $\mathbf{y}$  = local source position  
 $\alpha$  = turbulent velocity/convection velocity ratio  
 $\gamma$  = specific-heat ratio  
 $\delta_1$  = mixing-layer thickness, calculated as

$$\delta_1 = \int_{y_2=0}^{y_2^*} \left(1 - \frac{U_1}{U_{\text{axis}}}\right) dy_2$$

in which  $y_2^*$  is the radial location, where the velocity  $U_1 = 0.01 \times U_{\text{axis}}$

$\epsilon$  = dissipation rate of  $k$   
 $\theta$  = angle between the mean flow direction  $\mathbf{y}_1$  and the observer  $\mathbf{x}$   
 $\hat{\theta}$  = angle between the local source point  $\mathbf{y}$  and the observer  $\mathbf{x}$   
 $\Pi$  =  $l_n p$   
 $\rho$  = density  
 $\boldsymbol{\tau}$  = viscous stress tensor  
 $\tau_t$  = turbulence time scale  
 $\omega_t$  = turbulence angular frequency,  $\omega_t = 2\pi/\tau_t$

## Subscripts

$j$  = jet  
 $0$  = in the homogeneous medium at rest  
 $1$  = in the axial direction  
 $2$  = in the radial direction

## I. Introduction

PROGRESS in computational fluid dynamics (CFD) allows developments of new strategies for the calculation of acoustic fields radiated by turbulent flows. At least three approaches can be distinguished, each including a variety of methods for the representation of the flow, the acoustic sources, and the radiated sound (Fig. 1). The first class of methods relies on direct numerical simulation (DNS) in which the near acoustic field is obtained by solving the full compressible Navier-Stokes equations. Direct simulations of the aeroacoustics of fundamental configurations such as the scattering of sound waves by a vortex,<sup>1</sup> the radiated sound field of a vortex pair,<sup>2</sup> or a two-dimensional mixing layer<sup>3</sup> were carried out with success. However, DNS is limited for the moment to predictions of low-Reynolds-number jets. In a second group of methods the acoustic far field is evaluated in two steps through an acoustic analogy. First, the inner turbulent field is calculated; second, the acoustic far field is deduced by solving a wave equation. Two strategies are again possible with this approach. The near field can be obtained from a large eddy simulation (LES) or by synthesizing the fluctuating velocity field<sup>4-6</sup> from knowledge of the mean flow. These promising methods have been used to estimate the sound radiation from a box of isotropic turbulence<sup>7</sup> and the sound field radiated by a two-dimensional jet.<sup>8</sup> An alternative method combines the LES

Received Sept. 12, 1996; revision received April 25, 1997; accepted for publication July 7, 1997. Copyright © 1997 by the American Institute of Aeronautics and Astronautics, Inc. All rights reserved.

\*Assistant Professor, Laboratoire de Mécanique des Fluides et d'Acoustique, Centre National de la Recherche Scientifique 5509 and Ecole Centrale de Lyon, B.P. 163. Member AIAA.

†Scientist Engineer, Direction des Etudes et Recherches, 1 Avenue du Général de Gaulle. Member AIAA.

‡Professor of Fluid Mechanics, Laboratoire E.M2.C. du Centre National de la Recherche Scientifique et de l'Ecole Centrale Paris, Grande Voie des Vignes. Member AIAA.

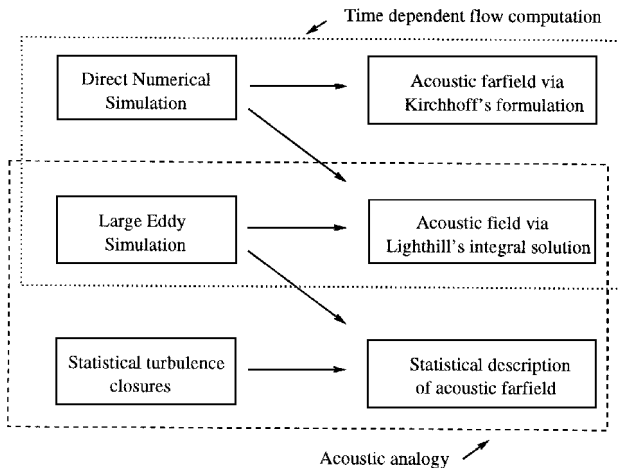


**Fig. 1** Some computational strategies for aerodynamic noise estimation.

calculation with a Kirchhoff integral representation of the acoustic far field. In the third group of methods, only the mean turbulent flow-field is calculated. Statistical source representations combined with a turbulence closure, such as the  $k$ - $\epsilon$  transport equations, then are used to predict the radiated acoustic far field of complex turbulent flows.

Our goal is to describe some recent developments and applications of the last group of methods to subsonic and supersonic jet noise. More precisely, although theoretical bases are now well established, it seems interesting to combine these results with available CFD tools to predict jet mixing noise.

One of the most elaborate statistical source models applicable to jet noise is that of Ribner.<sup>9</sup> A first combination of such a model with a numerical aerodynamic calculation is proposed by Hecht et al.<sup>10</sup> It is shown by Béchara et al.<sup>11</sup> that this approach yields good subsonic jet mixing noise estimates when data provided by a  $k$ - $\epsilon$  turbulence closure are introduced into the model. Because our goal is to develop predictive models, a global and unique adjustable factor is needed in these models, and this factor is adjusted on the basis of a single comparison with experimental data. This factor then is kept constant and used for all Mach numbers and all flow configurations, subsonic or supersonic round jets and coaxial jets. Thus, in the subsonic coaxial jet case, the ratio of the secondary exit velocity to the primary exit velocity, which minimizes the radiated acoustic power, is numerically determined by using the model as a black box. This approach has been extended to supersonic jet mixing noise.<sup>12,13</sup> The comparison of predicted results with experimental data shows a good agreement in the downstream direction, i.e.,  $0 \text{ deg} \leq \theta \leq 90 \text{ deg}$ . However, previous comparisons were less satisfactory in the second quadrant, i.e.,  $90 \text{ deg} \leq \theta \leq 180 \text{ deg}$ , and the difference between calculations and measurements increased with the nominal Mach number. The problem of obtaining reasonable predictions in the upstream direction was pointed out by Goldstein and Howes<sup>14,15</sup> many years ago, and these authors derived a convected wave equation for the pressure fluctuation. The main result of their analysis is a modification of the exponent  $-5$  of the Doppler or convection factor, which is replaced by an exponent  $-3$ . A simple comparison of the corresponding power law with measurements shows a better agreement when using the  $-3$  exponent (see Sec. II). An original contribution of the present study is to use a statistical description of turbulent fluctuations in combination with this acoustic analogy to improve supersonic mixing noise predictions. It is important to refine predictions in the upstream direction if one wishes to estimate the sound level during the launching of space vehicle systems. Indeed, although the radiated energy is higher for  $0 \text{ deg} \leq \theta \leq 90 \text{ deg}$ , acoustic energy radiated for  $\theta \geq 90 \text{ deg}$  directly affects vehicle components. Another possible advance in the same framework has been developed by Khavaran et al.<sup>18,19</sup> from Lighthill's analogy to compute refraction's effects in a jet at  $M = 1.4$ . Following the same line of reasoning, the Mach-wave noise component<sup>16</sup> can be evaluated from an analytical development of Ffowcs Williams and Maidanik.<sup>17</sup> This model has been applied to supersonic round jet at

$M = 2$  to predict the spectral peak as a function of the observer angle  $\theta$ .

This paper is organized as follows. Section II is devoted to Ribner's model, which is derived from a combination of Lighthill's analogy and an isotropic turbulence description. Using the same assumptions about turbulence description and the Goldstein-Howes<sup>14</sup> analogy, a new acoustic model is constructed in Sec. III. The acoustic analogy relies in this case on a convected wave equation that is shown to improve noise predictions in the case of high-speed jets. A model based on the work of Ffowcs Williams and Maidanik<sup>17</sup> is reviewed briefly in Sec. IV to estimate the Mach-wave noise component of the radiated acoustic far field. Aerodynamic results obtained with a  $k$ - $\epsilon$  turbulence closure are compared in Sec. V with available experimental data. Finally, the previous acoustic models are applied to shock-free subsonic and high-speed round jets. Comparison between measurements and numerical results are carried out for intensity, power spectral densities, and sound source localization.

## II. Ribner's Model

Lighthill's equation<sup>20</sup> is the starting point of this first model:

$$\frac{\partial^2 \rho'}{\partial t^2} - c_o^2 \frac{\partial^2 \rho'}{\partial x_i \partial x_i} = \frac{\partial^2 T_{ij}}{\partial x_i \partial x_j} \quad (1)$$

where the source term is defined as the fluctuating part of Lighthill's tensor  $T_{ij} = \rho u_i u_j + (p - c_o^2 \rho) \delta_{ij} - \tau_{ij}$ . In regarding  $\rho'$  as a variable, this inhomogeneous wave equation describes the sound propagation of a turbulence source volume in an external medium at rest. When the Reynolds number is high, of the order of  $10^4$ – $10^6$  as is the case in most practical applications, the viscous stress tensor can be neglected in the source term. Besides, for a perfect gas, fluctuations of pressure, density, and entropy are connected by  $p' = c_o^2 \rho' + (p_o/c_v) s'$ . Thus, acoustic generation and propagation without entropy fluctuations are such that  $p' = c_o^2 \rho'$  and Lighthill's tensor then is reduced with this assumption to  $T_{ij} = \rho u_i u_j$ . The exact solution to Eq. (1) for the density fluctuation is

$$\rho'(x, t) = \frac{1}{4\pi c_o^2} \int_V \frac{\partial^2 T_{ij}}{\partial y_i \partial y_j} [\mathbf{y}, t] \frac{d\mathbf{y}}{r} \quad (2)$$

where  $\mathbf{r} = \mathbf{x} - \mathbf{y}$  and the square brackets  $[\mathbf{y}, t]$  indicates that the corresponding expression is evaluated at the retarded time  $t - r/c_o$ . An equivalent form can be derived for the acoustic far field:

$$\rho'(x, t) = \frac{1}{4\pi c_o^4 x} \int_V \frac{r_i r_j}{r^2} \frac{\partial^2 T_{ij}}{\partial t^2} [\mathbf{y}, t] d\mathbf{y} \quad (3)$$

The acoustic intensity  $I(\mathbf{x})$  then is given by the autocorrelation function of the far-field acoustic fluctuations  $R_a(\mathbf{x}, \tau)$  evaluated at  $\tau = 0$ :

$$\begin{aligned} R_a(\mathbf{x}, \tau) &= \frac{\overline{\rho'(\mathbf{x}, t) \rho'(\mathbf{x}, t + \tau)}}{\rho_o c_o^{-3}} \\ &= \frac{A}{x^2} \frac{\partial^4}{\partial \tau^4} \iiint_V D_{ijkl} \mathcal{R}_{ijkl}(\mathbf{y}, \boldsymbol{\eta}, t) \delta\left(t - \tau - \frac{\mathbf{x} \cdot \boldsymbol{\eta}}{x c_o}\right) d\mathbf{y} d\boldsymbol{\eta} dt \end{aligned} \quad (4)$$

for a stationary turbulence, where the directivity tensor is expressed as  $D_{ijkl} = r_i r_j r_k r_l / r^4$ ,  $A = 1/16\pi^2 \rho_o c_o^5$  is a constant introduced to simplify the notations, and  $\mathcal{R}_{ijkl}$  is the fourth-order velocity correlation tensor in the far field:

$$\mathcal{R}_{ijkl}\left(\mathbf{y}, \boldsymbol{\eta}, \tau + \frac{\mathbf{x} \cdot \boldsymbol{\eta}}{x c_o}\right) \approx \overline{T_{ij}[\mathbf{y}, t] T_{kl}[\mathbf{y} + \boldsymbol{\eta}, t + \tau]}$$

Two velocity scales, namely the mean convection velocity  $U_c$  and the turbulent fluctuations  $u'$ , appear in the stress tensor correlation function. To identify the two effects of noise source mechanism and steady convection, a frame moving with the eddies mean convection velocity  $U_c$  is introduced. Furthermore, one assumes that turbulence is isotropic in this convected frame. The correlation function in the new reference frame takes the form

$$\mathcal{R}_{ijkl}(\mathbf{y}, \boldsymbol{\eta}, t) = R_{ijkl}(\mathbf{y}, \boldsymbol{\eta} - U_c t \mathbf{y}_1, \tau) = R_{ijkl}(\mathbf{y}, \boldsymbol{\xi}, t)$$

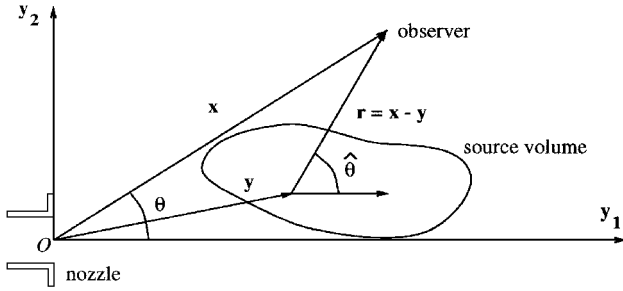


Fig. 2 Orientation of observation point relative to the mean flow.

The change of variables  $\xi = \eta - U_c t y_1$  and  $\lambda = \alpha U_c t$ , where  $\alpha U_c \sim u'$  is a typical turbulent velocity and  $\alpha$  is a small parameter, has been recently reformulated by Ffowcs Williams,<sup>21</sup> and leads for isotropic turbulence to

$$R_a(\mathbf{x}, \tau) = \frac{A}{x^2} \frac{1}{C^5} \iiint_V D_{ijkl} \frac{\partial^4}{\partial t^4} R_{ijkl}(\mathbf{y}, \xi, t) \delta\left(t - \frac{\tau}{C}\right) dy d\xi dt \quad (5)$$

where  $C$  is the Doppler or convection factor

$$C(M_c, \hat{\theta}) = [(1 - M_c \cos \hat{\theta})^2 + \alpha^2 M_c^2]^{\frac{1}{2}} \quad (6)$$

with  $\alpha^2 M_c^2 = \frac{\omega_i^2 L^2}{\pi c_o^2}$

and  $\hat{\theta}$  is the angle between the local source point  $\mathbf{y}$  and the observer  $\mathbf{x}$  (Fig. 2). At this step, note that a general calculation leads to a Doppler factor that is never singular.<sup>21</sup> Sound waves are produced by turbulent fluctuations and these sound waves are emitted more efficiently in the direction where the eddy velocity is equal to the speed of sound. This condition of Mach-wave noise,  $1 - M_c \cos \hat{\theta} = 0$ , corresponds to noncompact sources in the integral (4): The acoustic wavelength then is approximately given by the eddy length scale  $L$ , and the corresponding frequency  $c_o/L$  is lower than the characteristic turbulence frequency  $u'/L$ . Dimensional arguments then yield a power law for the sound field intensity over the entire Mach number range:

$$I(\mathbf{x}) \sim \frac{D^2 \rho_j^2}{x^2 \rho_o} \frac{U_c^3 M_c^5}{[(1 - M_c \cos \theta)^2 + \alpha^2 M_c^2]^{\frac{5}{2}}} \quad (7)$$

At supersonic convective Mach numbers, Mach waves are emitted in the direction defined by  $1 - M_c \cos \theta = 0$  and the acoustic power then is directly proportional to the jet mechanical power  $I(\mathbf{x}) \sim (D^2/x^2)(\rho_j^2/\rho_o)U_c^3$ . The acoustic radiation model can be deduced from Eq. (5) by following a procedure devised by Ribner.<sup>9</sup> The velocity field is first decomposed into a sheared mean flow and a fluctuating part  $u_i = U(y_2)\delta_{i1} + u'_i$ . In a second step, one introduces the previous velocity field description. The fourth-order correlation  $R_{ijkl}$  then appears as a sum of two contributions, namely the self-noise and the shear-noise<sup>22</sup>:

$$R_{ijkl}(\mathbf{y}, \xi, t) = \rho^2 [\overline{u'_i u'_j u'_k u'_l} + 4\delta_{1j} \delta_{1l} \overline{u'_i u'_k} U' U''] \quad (8)$$

In this expression, primed quantities are to be evaluated at  $[\mathbf{y}, t_o]$  and double primes indicate that quantities are to be evaluated at  $[\mathbf{y} + \xi, t_o + t]$ . One takes a Taylor expansion of  $U' U''$  around the midpoint  $\mathbf{y} + \xi/2$  to get  $U' U'' \simeq U^2 - (\xi_2^2/4)(dU/dy_2)^2$ . Assuming that the joint probability density for velocity components is normal,<sup>23</sup> one can write

$$\overline{u'_i u'_j u'_k u'_l} = \overline{u'_i u'_j} \overline{u'_k u'_l} + \overline{u'_i u'_k} \overline{u'_j u'_l} + \overline{u'_i u'_l} \overline{u'_j u'_k}$$

and the part of the function  $R_{ijkl}$  that contributes to the acoustic radiated field (the two last terms) can be finally expressed as a sum of second-order velocity correlations. A separation of space-time variables for this two-point velocity correlation then is postulated as  $R_{11} = R(\xi)g(\tau)$  and the spatial factor for an isotropic turbulence is given by

$$R(\xi) = u^2 \left[ \left( f + \frac{1}{2} \xi \frac{df}{d\xi} \right) \delta_{ij} - \frac{1}{2} \frac{df}{d\xi} \frac{\xi_i \xi_j}{\xi} \right]$$

In this expression,  $f(\xi)$  designates the longitudinal correlation function. This function is assumed to be Gaussian  $f(\xi) = \exp(-\pi \xi^2/L^2)$ , where  $L$  is the local integral scale in the axial direction. Usually, a Gaussian time correlation function  $g(\tau)$  is chosen.<sup>9,13</sup> As pointed out by Ribner,<sup>9</sup> to calculate the power spectral density and the acoustic intensity given by  $I(\mathbf{x}) = R_a(\mathbf{x}, \tau = 0)$ , the two quantities  $d^4 g/d\tau^4$  and  $d^4 g^2/d\tau^4$  must be defined at  $\tau = 0$ . In the present paper, the Gaussian correlation is replaced by the following function to improve the low-frequency predictions (see Sec. V):

$$g(\tau) = \frac{1}{\cosh(\beta \omega_i \tau)} \quad (9)$$

where  $\beta = \frac{2}{5}$  is adjusted<sup>24</sup> to fit the experimental data of Davies et al.<sup>25</sup> Then, the first space integration in Eq. (5) is carried out with respect to  $\xi$ . Assuming constant mean flow quantities over the correlated volume, one finds

$$I(\mathbf{x}) = \frac{A}{x^2} \int_V \left\{ \frac{\rho^2 L^3 u'^4 L^3}{2\sqrt{2} C^5} \frac{d^4 g^2}{d\tau^4} \Big|_{\tau=0} + \frac{\rho^2 L^5 u'^2}{2\pi C^5} \left( \frac{dU}{dy_2} \right)^2 D_\theta \frac{d^4 g}{d\tau^4} \Big|_{\tau=0} \right\} dy \quad (10)$$

for the acoustic intensity, where  $D_\theta = (\cos^4 \hat{\theta} + \cos^2 \hat{\theta})/2$  is the directivity of the shear noise. Expression (10) of the acoustic intensity indicates that the self-noise directivity is isotropic, whereas the shear-noise pattern features a dipolar shape. One takes the Fourier transform of the correlation function  $R_a$  to get the power spectral density  $S_a$ :

$$S_a(\mathbf{x}, \omega) = \frac{A}{x^2} \int_V (S_a^{sf} + S_a^{sh}) dy \quad (11)$$

where the two components are given by

$$S_a^{sf} = \frac{\rho^2 L^3 u'^4 \omega^4}{2\sqrt{2}} \frac{1}{\omega_i \beta \pi} \frac{1}{\sinh[(\pi/2\beta)(C\omega/\omega_i)]}$$

$$S_a^{sh} = \frac{\rho^2 L^5 u'^2 D_\theta}{2\pi} \left( \frac{dU_1}{dy_2} \right)^2 \frac{\omega^4}{\omega_i} \frac{1}{2\beta} \frac{1}{\cosh[(\pi/2\beta)(C\omega/\omega_i)]}$$

and correspond respectively to self- and shear-noise sources. The last expression (11) describes the space-frequency distribution of acoustic sources in a turbulent flow. Applications of this model presented in Sec. V indicate that it is inaccurate in the upstream direction,  $90 \text{ deg} \leq \theta \leq 180 \text{ deg}$ , when the jet Mach number takes large values. The problem was pointed out by Goldstein and Howes<sup>14,15</sup> and others many years ago, and it is illustrated in Fig. 3.

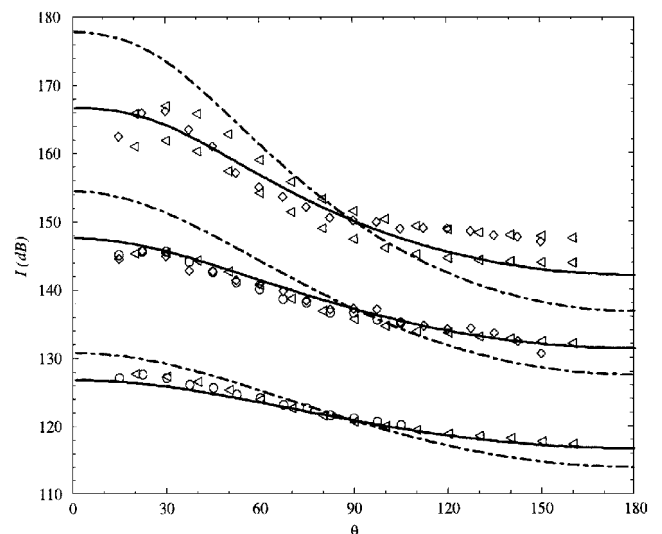


Fig. 3 Directivity for three Mach numbers:  $M = 0.56, 0.86,$  and  $1.34$ . Power law: —, Doppler factor at power  $-3$  ---, Doppler factor at power  $-5$  (Lighthill's theory). Experimental data:  $\triangle$ , SAE<sup>35</sup>;  $\circ$ , Lush<sup>30</sup>; and  $\diamond$ , Tanna et al.<sup>31</sup>

Because Lighthill's analogy relies on a wave operator of a homogeneous medium at rest, it does not suitably account for acoustic wave convection. Indeed, the source convection is modeled through the Doppler factor  $C$  with an exponent of  $-5$ . Ribner's model was generalized by Goldstein and Rosenbaum,<sup>26</sup> who assumed an axisymmetric turbulence field in the moving frame. Béchara et al.<sup>11</sup> have applied this model to subsonic jet noise and coaxial jet noise and obtained adequate noise radiation predictions. However, the difficulty in this approach is that one has to describe turbulence anisotropy by prescribing the ratio between the transverse and the longitudinal integral scales. One often assumes that the longitudinal integral length scale is three times the transverse scale. In the present work, this model is not retained for supersonic flows in which the ratio of turbulence length scale is not well known and not directly provided by mean-flow aerodynamic calculations.

### III. Goldstein–Howes Model

To deal with high-Mach-number configurations, one may use the alternate theory of Goldstein–Howes.<sup>14</sup> The model relies on a convected wave equation. The aerodynamic sources then are described as in Ribner's analysis. As a starting point, the dynamic equations are written in terms of the logarithm of the pressure  $\Pi = \ln p$ . This yields the Lilley<sup>27,14</sup> wave equation, which may be written as

$$\begin{aligned} & \frac{D}{Dt} \left\{ \frac{D^2 \Pi}{Dt^2} - c_o^2 \frac{\partial^2 \Pi}{\partial x_i \partial x_i} \right\} - 2\gamma \frac{dU}{dx_2} \frac{\partial}{\partial x_1} \left( \frac{Du'_2}{Dt} \right) \\ & = \gamma \frac{D}{Dt} \left( \frac{\partial u'_i}{\partial x_j} \frac{\partial u'_j}{\partial x_i} \right) \end{aligned} \quad (12)$$

where  $D/Dt = \partial/\partial t + U\partial/\partial x_1$  is the material derivative along the sheared mean flow. One only assumes that the turbulent velocity field contributes to the radiated acoustic field as in Ribner's model. One of the key issues in acoustic analogy modeling is to identify source terms. The left-hand side of Eq. (12) is the exact wave operator that one can derive from linearized equations of motion in the case of parallel mean flows. A more suitable form of the wave equation (12) can be obtained<sup>14,15</sup> by assuming that the turbulent fluctuation field  $\mathbf{u}'$  is incompressible and by considering that  $d^2U/dx_2^2$  can be neglected:

$$\frac{D^2 \Gamma}{Dt^2} - c_o^2 \nabla^2 \Gamma = \gamma \frac{\partial^2}{\partial x_i \partial x_j} \left( \frac{Du'_i u'_j}{Dt} \right) + 4\gamma \frac{\partial}{\partial x_1} \left( \frac{dU}{dx_2} \frac{Du'_2}{Dt} \right) \quad (13)$$

where  $\Gamma = D\Pi/Dt$ . This equation is interpreted in the frame of an acoustic analogy as Lighthill's equation (1). The left-hand side of Eq. (13) is Phillips' operator applied to  $\Gamma$ , and the right-hand side is an acoustic source term expressed in terms of turbulent velocity components. Goldstein and Howes<sup>14</sup> give an approximate solution of Eq. (13) valid in the low-frequency range. Besides, in the far field where the medium is at rest,  $\Gamma$  takes an especially simple form  $\Gamma \simeq (\gamma/\rho_o c_o^2) \partial p'/\partial t$  and, finally, the power spectral density  $S_a$  per unit source volume takes the following form:

$$\begin{aligned} S_a(\mathbf{x} | \mathbf{y}, \omega) &= \frac{A\omega^4 C^2}{2\pi x^2} \left\{ \iint R_{1111} e^{iC\omega\tau} d\tau d\xi \right. \\ & \left. - D_\theta \frac{16}{3} \left( \frac{dU}{dy_2} \right)^2 \iint \xi_2^2 R_{11} e^{iC\omega\tau} d\tau d\xi \right\} \end{aligned} \quad (14)$$

From this last expression, one may develop an isotropic turbulence modeling to estimate the two velocity correlations  $R_{1111}$  and  $R_{11}$ . After some lengthy calculations, one finds the power spectral density expression corresponding to Eq. (14) for a Gaussian time correlation function  $g(\tau)$ :

$$\begin{aligned} S_a(\mathbf{x}, \omega) &= \frac{1}{8\pi^3 \sqrt{\pi} \rho_o c_o^5 x^2} \int_V \frac{\rho^2 u^2 L^3}{\omega_i} \omega^4 \left\{ \frac{u^2 C^2}{16} \exp\left(-\frac{C^2 \omega^2}{8\omega_i^2}\right) \right. \\ & \left. + \frac{L^2 C^2}{3\pi} \left( \frac{\partial U}{\partial y_2} \right)^2 \exp\left(-\frac{C^2 \omega^2}{4\omega_i^2}\right) D_\theta \right\} dy \end{aligned} \quad (15)$$

and the acoustic intensity  $I(\mathbf{x}) = R_a(\mathbf{x}, \tau = 0)$  is obtained by taking the Fourier transform of  $S_a(\mathbf{x}, \omega)$

$$I(\mathbf{x}) = \frac{1}{\pi^3 \rho_o c_o^5 x^2} \int_V \frac{\rho^2 u^2 L^3 \omega_i^4}{C^3} \left\{ \frac{3u^2}{2\sqrt{2}} + \frac{L^2}{\pi} \left( \frac{\partial U}{\partial y_2} \right)^2 D_\theta \right\} dy \quad (16)$$

The acoustic intensity appears again as the sum of two contributions, turbulence interaction with itself and turbulence interaction with the mean flow. The two associated directivities are identical with those found in Lighthill's analogy. However, the convection factor  $C^{-5}$  now is replaced by the same Doppler factor at the power  $-3$ . This notably improves the predicted directivity for supersonic Mach numbers. The ratio of the shear-noise taken at  $\hat{\theta} = 0$  to the self-noise is  $1/2\sqrt{2\pi}$  for Lighthill's model and  $2\sqrt{2}/3\pi$  for the Goldstein–Howes model. Thus, the relative importance of the shear-noise component is higher in the second approach.

### IV. Mach-Wave Noise Model

When the convection Mach number takes supersonic values, the velocity  $U_c$  may become equal to the speed of sound in the observer direction, and in this case, the acoustic field associated with this turbulent source volume convected at  $U_c$  is radiated with great efficiency (Fig. 4). In this section, we briefly present a Mach-wave noise model that only evaluates this component of the sound field. The complete model relies on an analytical development by Ffowcs Williams and Mairdani<sup>17</sup>. Detailed analysis of this model can be found in Ref. 16. As in the two previous models, expressions are derived for the Mach-wave noise intensity,

$$I_M(\mathbf{x}) = \frac{c_o^2 p_o^2}{32\pi^2 \rho_o x^2} \int_{V^*} \frac{\cos^2 \hat{\theta} \sin^2 \hat{\theta}}{\tilde{C}^5} \left[ \frac{1}{c^2} \frac{dU}{dy_2} \right]^2 M_c^3 \tau_i dy \quad (17)$$

and for the associated power spectral density,

$$S_{aM}(\mathbf{x}, \omega) = \frac{p_o^2}{32\pi^2 \rho_o} \int_{V^*} \frac{\cos^2 \hat{\theta} \sin^2 \hat{\theta}}{\tilde{C}^5} \omega^2 G(\omega) \tau_i \delta_1^2 M_c dy \quad (18)$$

where  $\tau_i$  is the turbulence time decay and  $\delta_1$  designates the mixing-layer thickness. The integration is performed over the source volume  $V^*$ , defined as the set of points in the flow for which the convection Mach number exceeds unity  $V^* = \{y \in V, M_c(y) > 1\}$ , and  $\tilde{C}$  designates a normalized convection factor  $\tilde{C} = C/\alpha M_c$ . The function  $G$

$$G(\omega) = \left[ 1 - \frac{5}{8} \left( 1 - \frac{\omega^2}{2\omega_M^2} \right) \right] \frac{1}{2\sqrt{\pi} \omega_M} \exp\left(-\frac{\omega^2}{4\omega_M^2}\right)$$

is the Fourier transform of the pressure autocorrelation<sup>28</sup>  $g$  with  $p'p''(\boldsymbol{\eta}, \tau) = \overline{p'p''(\boldsymbol{\eta}, 0)g(\tau)}$ , and the angular frequency  $\omega_M$  is given by  $\omega_M^2 = 2U_c^2/9\delta_1^2$ . Expression (18) is specifically derived for Mach-wave radiation and provides the space-frequency distribution of this special type of noise emission.

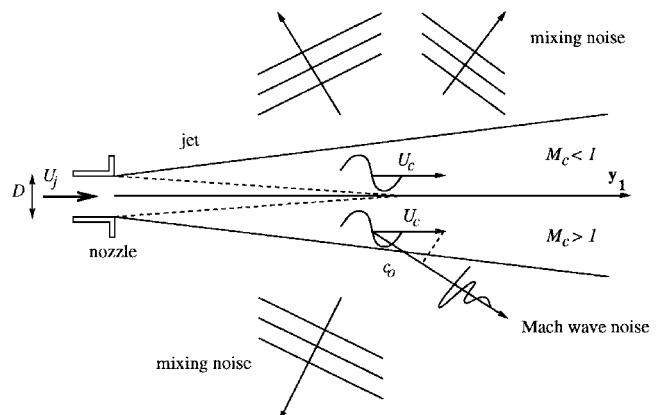


Fig. 4 Sketch of jet radiation.

## V. Some Applications to Jet Noise

### A. Aerodynamic Results

Knowledge of the mean flowfield through such statistical quantities as the mean flow gradient  $dU/dy_2$ , the sound speed  $c$ , or the convection Mach number  $M_c$  on the one hand and the turbulence time scale  $\tau_t$  and the turbulence longitudinal length scale  $L$  on the other hand allows the power spectral density to be computed by integration of expressions (11), (16), and (18). All of these quantities can be deduced from an aerodynamic calculation using a turbulence closure such as the compressible  $k-\epsilon$  model. The effect that compressibility has on turbulence is taken into account through an energy dissipation resulting from dilatation processes.<sup>29</sup> A description of the turbulence model is given in Appendix A, and some results are provided in the literature.<sup>13,16</sup>

In Fig. 5, the calculated mean centerline velocity is compared to data of Seiner et al.<sup>33</sup> for a free jet at  $M = 2$  and for two temperatures,  $T_j/T_o = 1$  and 2.8. The faster decrease of the velocity with increasing jet temperature is well retrieved by the calculation. The small wiggles for the predicted hot-jet profile are due to a slight mismatch between the jet exit pressure and the ambient pressure. The radial profiles for several axial locations are plotted in Fig. 6 in the case of a jet at  $M = 2$  and a  $T_j/T_o = 1$ . The calculated profiles collapse on the fitted curve provided by Seiner et al.<sup>34</sup> The jet spreading rate for the same jet flow is compared to measurements<sup>33</sup> in Fig. 7, and the radial profiles of turbulence intensity are plotted in Fig. 8. The maximum is reached for a reduced coordinate (see definition in the caption)  $\eta \approx -0.1$ . Thus, the maximum intensity is around  $y_2 = D/2$ , and it reaches about 11% of the jet exhaust velocity.

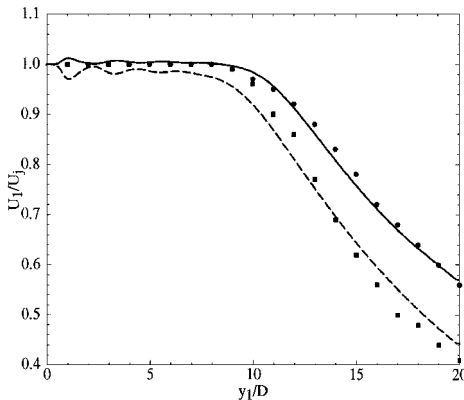


Fig. 5 Mean axial velocity for a free jet at Mach 2. Calculations:  $\bullet$ ,  $T_j/T_o = 1$  and  $\blacksquare$ ,  $T_j/T_o = 2.8$ . Data of Seiner et al.<sup>33</sup>: —,  $T_j/T_o = 1$  and ---,  $T_j/T_o = 2.8$ .

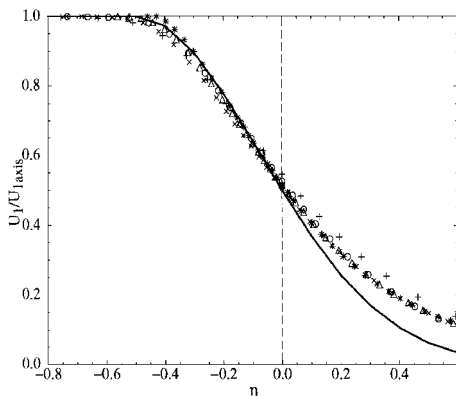


Fig. 6 Radial velocity profiles of a jet at  $M = 2$  and  $T_j/T_o = 1$ . Calculations:  $+$ ,  $y_1 = 3D$ ;  $\circ$ ,  $y_1 = 5D$ ;  $\times$ ,  $y_1 = 7D$ ;  $\triangle$ ,  $y_1 = 9D$ ;  $*$ ,  $y_1 = 11D$ ; and —, measurements of Seiner et al.<sup>34</sup> fitted to a half-Gaussian. The variable  $\eta$  is defined as  $\eta = [y_2 - y_2(0.5)]/\delta$ , where  $y_2(0.5)$  is the radial location where the velocity equals  $U_1 = 0.5U_{1,axis}$  and  $\delta$  is the local shear-layer thickness  $\delta = y_2(0.1) - y_2(0.9)$ , which represents the radial distance between the points where the local velocity is  $U_1 = 0.1U_{1,axis}$  and  $U_1 = 0.9U_{1,axis}$ .

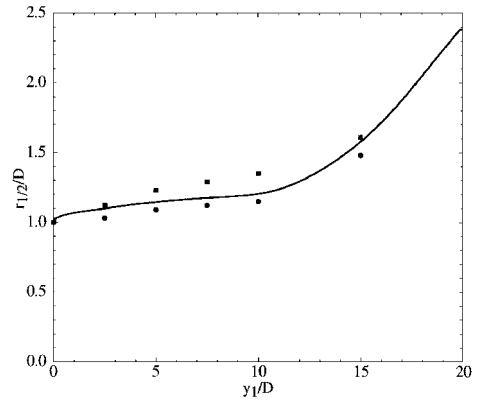


Fig. 7 Normalized radius  $r_{1/2}/D$  to half velocity, defined as the radial distance, where  $U_1 = 0.5 \times U_{axis}$ , for a jet at  $M = 2$  and  $T_j/T_o = 1$ . Calculations: —, data of Seiner et al.<sup>33</sup>;  $\blacksquare$ ,  $T_j/T_o = 0.62$ ; and  $\bullet$ ,  $T_j/T_o = 1.51$ .

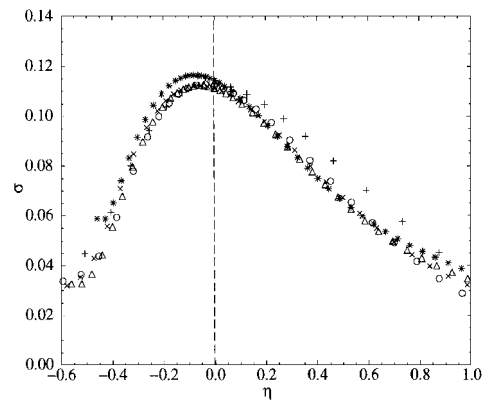


Fig. 8 Turbulence intensity profiles of a jet at  $M = 2$  and  $T_j/T_o = 1$ . Calculations:  $+$ ,  $y_1 = 3D$ ;  $\circ$ ,  $y_1 = 5D$ ;  $\times$ ,  $y_1 = 7D$ ;  $\triangle$ ,  $y_1 = 9D$ ; and  $*$ ,  $y_1 = 11D$ . The turbulence intensity  $\sigma$  is defined as  $\sigma = u'_1/U_{axis}$ .

### B. Acoustic Results

The following closures are used in the three mixing-noise models. First, turbulence local characteristics are approximated by  $\omega_l = 2\pi\epsilon/k$  for the angular frequency,  $\tau_t = k/\epsilon$  for the time scale, and  $L = k^{3/2}/\epsilon$  for the turbulence integral longitudinal length scale. The convection velocity  $U_c$  is not a primitive variable of the aerodynamic calculation. In agreement with many experimental observations, we choose to take a constant convection velocity in each transverse section with a value determined by the local mean axis velocity  $U_c(y_1) = 0.67 \times U_{axis}(y_1)$ .

The three models use quantities that depend implicitly on unknown scaling constants. An adjustable multiplicative constant is also necessary in the expression of the acoustic intensity. This single global factor is determined by comparison with experimental data obtained by Lush<sup>30</sup> for the first two models at the point  $M = 0.56$  and  $\theta = 90$  deg. In the case of the Mach-wave noise model, the reference point is provided by Tanna et al.,<sup>31</sup> Tanna,<sup>32</sup> and Seiner et al.<sup>33</sup> for a jet at  $M = 2$  and  $T_j/T_o = 1$  and an observation angle  $\theta = 39$  deg. This angle corresponds to the maximum of the directivity pattern. The constants determined in this way are used without further adjustment to deal with all other flow configurations. Acoustic levels for directivity and narrow-band spectra, are always given per unit of nozzle area and corrected to the distance  $x$  of the observer, with a reference of  $I_o = 10^{-12}$  W/m<sup>2</sup>.

Figure 9 shows the acoustic directivity of a  $M = 0.56$  and  $T_j/T_o = 1$  jet as a function of the observation angle  $\theta$ . The two mixing noise models (10) and (16) are plotted and are compared with data of Lush<sup>30</sup> and with Society of Automotive Engineers (SAE)<sup>35</sup> correlations. The angle  $\theta = 90$  deg is taken as reference and the models are used without further adjustment. The difference between calculations and experimental data may reach up to 6 dB at small angles for Ribner's model and 4 dB at very large

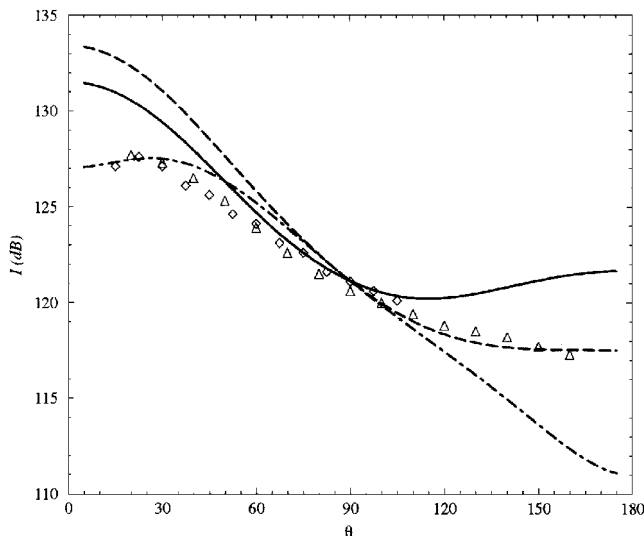


Fig. 9 Jet at  $M = 0.56$  and  $T_j/T_o = 1$ , acoustic directivity in decibels as a function of the outlet angle  $\theta$ : —, Goldstein-Howes model (16); ---, Ribner's model (10); - · -, Goldstein-Rosenbaum model<sup>11</sup>;  $\diamond$ , Lush<sup>30</sup> data; and  $\triangle$ , SAE data.<sup>35</sup>

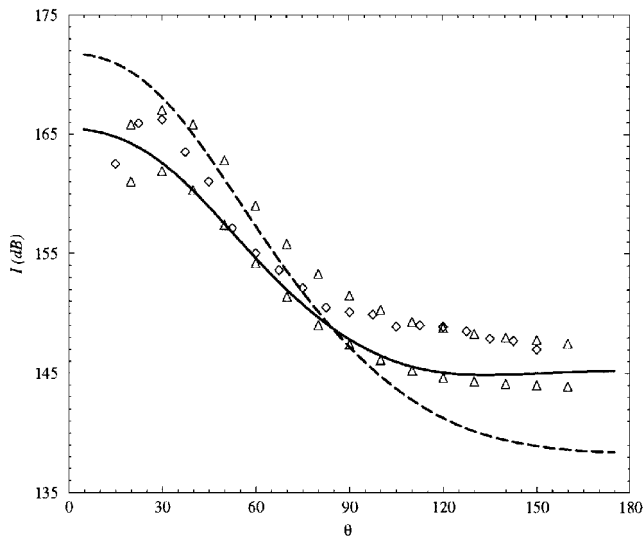


Fig. 10 Jet at  $M = 1.34$  and  $T_j/T_o = 1$ , acoustic directivity in decibels as a function of the outlet angle  $\theta$ : —, Goldstein-Howes model (16); ---, Ribner's model (10);  $\diamond$ , Tanna et al.<sup>31</sup> data; and  $\triangle$ , SAE data<sup>35</sup> for a jet at  $M = 1.26$  and  $1.41$ .

angles for the Goldstein-Howes model. The predicted intensity is not improved by this model in this case. Results calculated by Goldstein and Rosenbaum<sup>11,26</sup> also are displayed. The difference between this model and measurements is much higher than that corresponding to the other two models in the upstream direction. The jet at  $M = 1.34$  and  $T_j/T_o = 1$  is an interesting case at this step of the discussion. Indeed, comparisons between calculations and measurements show that the acoustic intensity is more accurately predicted with the Goldstein-Howes model (Fig. 10), which closely follows data in particular in the upstream direction. Moreover, the difference between the two models is of the order of 7 dB in this direction. The case of a perfectly expanded jet at  $M = 2$  also has been investigated (Fig. 11). The Mach-wave noise model predictions are close to the data of Seiner et al.<sup>33</sup> when this component dominates the sound field, i.e., for  $20 \text{ deg} \leq \theta \leq 60 \text{ deg}$ . However, for angles higher than  $\theta = 60 \text{ deg}$ , the mixing noise is the main component of the acoustic field and the Goldstein-Howes model retrieves the experimental data, unlike Ribner's model. The dropoff observed in experimental intensity at small angles is caused by refraction effects, which are not modeled here. These effects are often difficult to measure. Moreover, it seems that the Mach-wave noise component

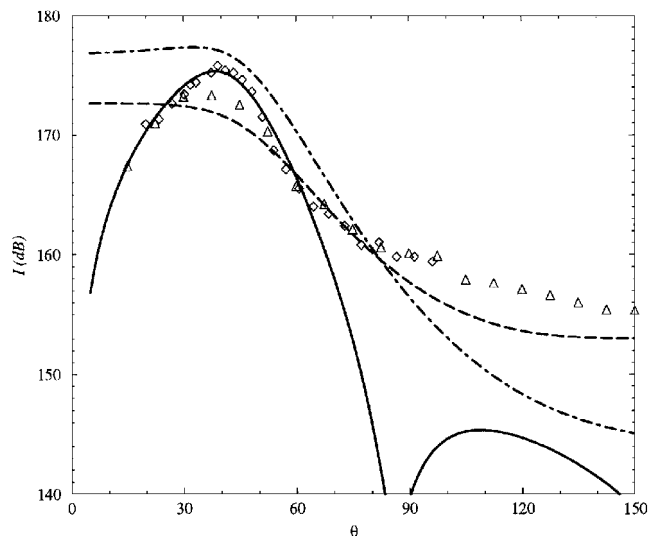


Fig. 11 Jet at  $M = 2.0$  and  $T_j/T_o = 1$ . Acoustic directivity in decibels as a function of the outlet angle  $\theta$ : —, Mach-wave model (17); ---, Goldstein-Howes model (16); - · -, Ribner's model (10).  $\diamond$ , Seiner et al.<sup>33</sup> data and  $\triangle$ , Tanna et al.<sup>31</sup> data for a jet at  $M = 1.95$  and  $T_j/T_o = 1$ .

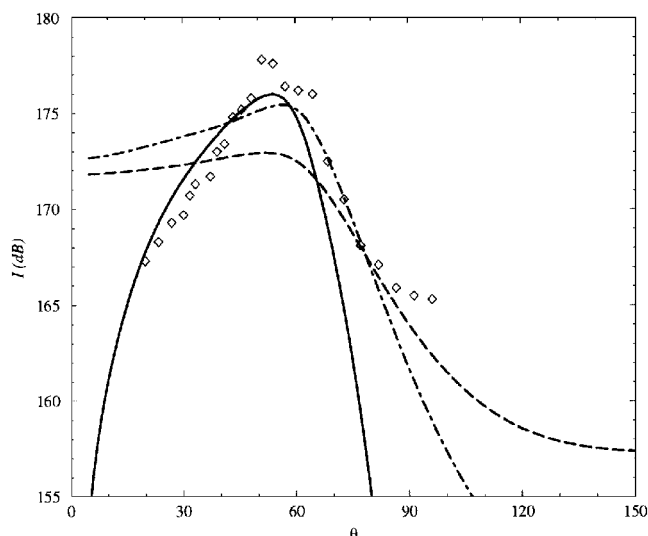
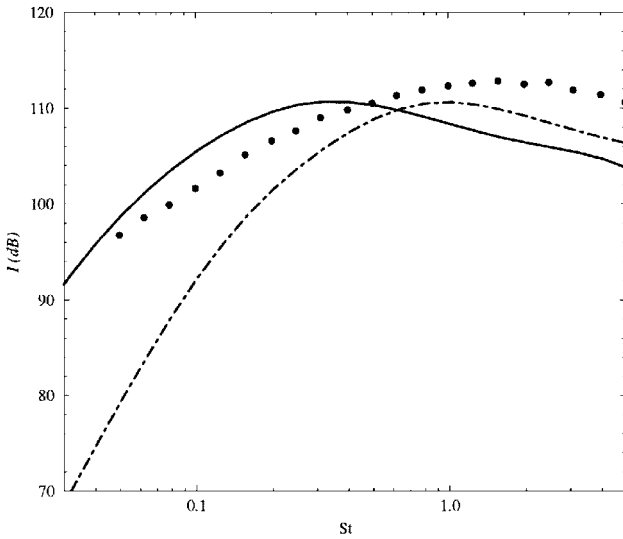


Fig. 12 Jet at  $M = 2.0$  and  $T_j/T_o = 2.8$ , acoustic directivity in decibels as a function of the outlet angle  $\theta$ : —, Mach-wave model (17); ---, Goldstein-Howes model (16); - · -, Ribner's model (10);  $\diamond$ , Seiner et al.<sup>33</sup> data.

imposes the directivity pattern at small angles for this case, and this explains the correct agreement between calculations and measurements. The mixing-noise component given by Eq. (10) or (16) does not contain the Mach-wave noise, in contrast with expression (7). By using the previous description of an isotropic turbulence and by integrating with respect to  $\xi$  over the correlated volume, these two models treat compact sources. To conclude on this point, a correct estimation of the radiated acoustic field is obtained by taking the Mach-wave noise component for  $\theta \leq 60 \text{ deg}$ , where this component dominates the sound field, and the mixing-noise contribution for  $\theta \geq 60 \text{ deg}$ . To validate this interpretation, a jet at  $M = 2$  and  $T_j/T_o = 2.8$  is analyzed in the same way (Fig. 12). The peak of intensity now is given by  $\theta^* \approx \cos^{-1}(1/M_c) \approx 51 \text{ deg}$ . Note that the Mach-wave noise component is retrieved. The mixing noise predicted by the Goldstein-Howes model again provides improved estimates for higher angles of observation,  $\theta > 70 \text{ deg}$ .

Third-octave spectra are compared to mixing noise data of Tanna et al.<sup>31</sup> in Ref. 13. This first attempt gave results that required some improvement. This is done here using the new time correlation (9) defined in Sec. II. To obtain adequate spectral predictions, it is important to refine the modeling of the time-correlation function  $g(\tau)$ .



**Fig. 13** Third-octave band spectra of a jet at  $M = 0.56$  and  $T_j/T_o = 1$  at  $\theta = 90$  deg: —, Ribner's model (11) with the new time correlation function (9); - - -, Ribner's model with a Gaussian time correlation<sup>13</sup>; and •, data of Tanna et al.<sup>31</sup> for a jet at  $M = 0.60$ .

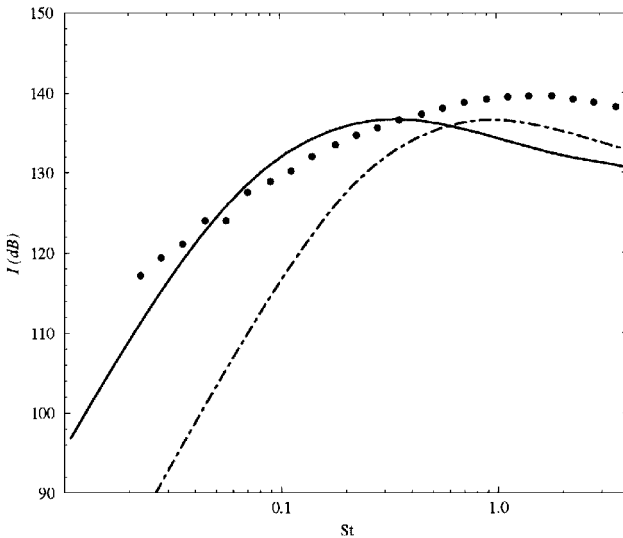


**Fig. 14** Third-octave band spectra of a jet at  $M = 1.34$  and  $T_j/T_o = 1$  at  $\theta = 90$  deg: —, Ribner's model (11) with the new time correlation function (9); - - -, Ribner's model with a Gaussian time correlation<sup>13</sup>; and •, data of Tanna et al.<sup>13</sup>

To save space, we only show results corresponding to an observation angle  $\theta = 90$  deg and two Mach numbers,  $M = 0.56$  and  $1.34$ . Figures 13 and 14 display the experimental estimates, previous predictions based on a Gaussian correlation function,<sup>13</sup> and present results obtained with the new correlation expression (9). Agreement is satisfactory. The differences are found in the high-frequency range and can be attributed to the difficulty of adjusting the correlation function and possibly to experimental imperfections in the spectral estimations. Agreement also is obtained for other angles of observation except in the directions close to the jet axis ( $\theta \approx 0$  deg), where refraction effects are important. Mach-wave noise component can be plotted in various ways. Figure 15 displays the calculated angular distribution for a set of Strouhal numbers for a high-speed hot jet. The figure also includes the data of Seiner et al.<sup>33</sup> and the predictions of Tam and Chen<sup>36</sup> for the same case. Calculated results are relatively close to the measured distributions. Both predictions feature the same precision. In the case of hot jets, our method yields accurate results.<sup>16</sup>

Figure 16 gives another point of view in displaying the relative power spectral density per unit length along the jet axis vs the dimensionless axial position  $y_1/D$  and the apparent Strouhal number

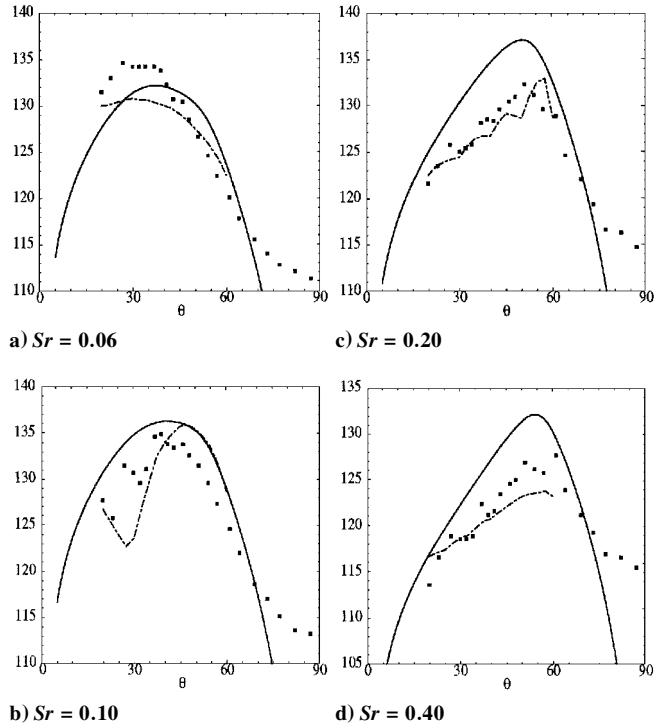


**Fig. 15** Directivity of Mach-wave noise in decibels, for a jet at  $M = 2$  and  $T_j/T_o = 2.3$ : ■, Seiner et al.<sup>33</sup> data; —, present Mach-wave noise model (18); and - - -, Tam-Chen calculations.<sup>36</sup>

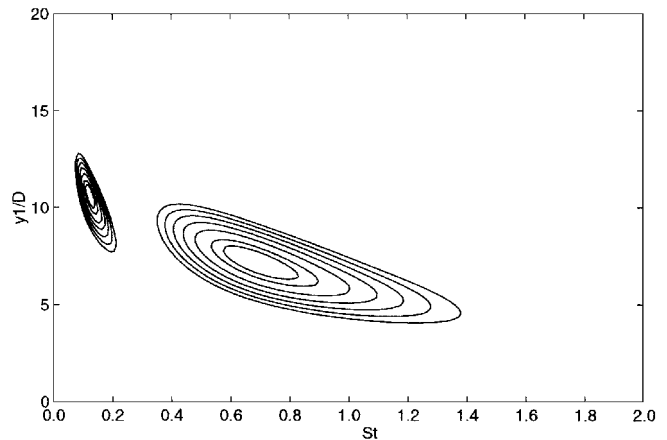


**Fig. 16** Jet at  $M = 2$  and  $T_j/T_o = 1$ , observer angle  $\theta = 39$  deg. Isocontours of the calculated relative acoustic power per unit length along the jet axis as a function of the dimensionless axial position  $y_1/D$  and the dimensionless apparent frequency  $Sr = fU_j/D$ . The Mach-wave noise component is located at  $y_1/D = 10.5$  and  $Sr = 0.12$ , whereas the mixing-noise component is located at  $y_1/D = 4.9$  and  $Sr = 0.67$ .

$Sr$ . The mixing-noise component (11) and the Mach-wave noise component (18) are shown for the case of a jet at  $M = 2$  and  $T_j/T_o = 1$ , and for an observation angle  $\theta^* = \cos^{-1}(1/M_c) \approx 39$  deg, corresponding to the Mach-wave direction. In general, the low-frequency sources are located in the developed region, whereas the high-frequency sources are situated in the mixing region near the nozzle. In the present case, the maximum of the Mach wave source is located at  $y_1/D \approx 10.5$  and  $Sr \approx 0.12$ , whereas the maximum of the mixing-noise source is predicted at  $y_1/D \approx 4.9$  and  $Sr \approx 0.67$ . The acoustic source distribution has two peaks, with a low-frequency peak situated near the end of the potential core ( $X_c \approx 10D$ ) of the jet.

### VI. Concluding Remarks

This article describes some aeroacoustic model developments based on extensions of Lighthill's theory.<sup>20</sup> Applications to subsonic and supersonic jet noise are carried out. Noise-level estimation is

based on a statistical model coupled with an integral solution of a wave equation. Estimates of acoustic radiation are obtained for the different components of the sound field, including Mach waves. Two of the models improve predictions of the supersonic mixing noise. Because the goal is to develop prediction methods, only one adjustable factor is used for each of them. Angular intensity distribution and spectral estimates are in general agreement with experimental data, but the method has several limitations. First, it requires knowledge of Green's function and is essentially applicable to free-space radiation problems. Second, refraction effects by the mean flow gradients are not taken into account. Third, entropy sources that may be important in the hot-jet case are not modeled. Further validations of these statistical methods will require comparisons between calculated and measured source distributions.

### Appendix: Turbulence Model

The aerodynamic fields are obtained from a numerical solution of the Favre-averaged Navier-Stokes equations with a compressible  $k-\epsilon$  turbulence closure. Using the Favre average for each variable,  $\phi = \bar{\phi} + \phi'' = \overline{\rho\phi}/\bar{\rho} + \phi''$ , except for the density  $\rho$  and the pressure  $p$ , one can write the mean flowfield equations as follows:

$$\frac{\partial \bar{\rho}}{\partial t} + \frac{\partial (\bar{\rho} \bar{u}_i)}{\partial x_i} = 0 \quad (\text{A1})$$

$$\bar{\rho} \left( \frac{\partial \bar{u}_i}{\partial t} + \bar{u}_j \frac{\partial \bar{u}_i}{\partial x_j} \right) = - \frac{\partial \bar{p}}{\partial x_i} + \frac{\partial}{\partial x_j} (\bar{\tau}_{ij} - \overline{\rho u_i'' u_j''}) \quad (\text{A2})$$

$$\begin{aligned} \bar{\rho} \left( \frac{\partial \bar{h}}{\partial t} + \bar{u}_j \frac{\partial \bar{h}}{\partial x_j} \right) &= \frac{\partial}{\partial x_j} \left( \frac{\lambda}{c_p} \frac{\partial \bar{h}}{\partial x_j} - \overline{\rho u_j'' h''} \right) + \frac{\partial \bar{p}}{\partial t} \\ &+ \bar{u}_j \frac{\partial \bar{p}}{\partial x_j} + \left\{ \bar{u}_j \frac{\partial \bar{p}}{\partial x_j} + \overline{u_j'' \frac{\partial \bar{p}}{\partial x_j}} + \bar{\Phi} \right\} \end{aligned} \quad (\text{A3})$$

where  $-\overline{\rho u_i'' u_j''}$  is the Reynolds stress tensor and  $\tau_{ij}$  is the viscous stress tensor, which takes the following form for a compressible Newtonian fluid:

$$\bar{\tau}_{ij} = \mu \left( \frac{\partial \bar{u}_i}{\partial x_j} + \frac{\partial \bar{u}_j}{\partial x_i} \right) - \frac{2}{3} \mu \frac{\partial \bar{u}_k}{\partial x_k} \delta_{ij}$$

In the specific-enthalpy equation (A3),  $\lambda$  is the heat conductivity,  $c_p$  is the specific heat at constant pressure, and  $\Phi$  is the viscous dissipation function  $\Phi = \tau : \nabla \mathbf{u}$ . One assumes Fourier's law for the heat-flux vector  $\mathbf{q} = -\lambda \nabla T$  and a perfect gas behavior  $dh = c_p dT$ . The term  $-\overline{\rho u_j'' h''}$  is modeled by means of a gradient closure,

$$-\overline{\rho u_j'' h''} \approx \frac{\mu_t}{\sigma_t} \frac{\partial \bar{h}}{\partial x_j}$$

In this expression,  $\mu_t$  is the turbulent viscosity and  $\sigma_t$  is the turbulent Prandtl number. The three last terms (in braces) of the enthalpy equation (A3) are neglected in the numerical solution. Compressibility effects on turbulence have been taken into account through an energy dissipation<sup>29</sup> resulting from dilatation processes. In its final form, the  $k-\epsilon$  turbulence model describes the mass weighted kinetic energy and dissipation:

$$k = \frac{1}{2} \overline{u_i'' u_i''} = \frac{1}{2} \frac{\overline{\rho u_i'' u_i''}}{\bar{\rho}} \quad \bar{\rho} \epsilon = \overline{\tau_{ij}'' \frac{\partial u_i''}{\partial x_j}}$$

The dissipation  $\epsilon$  of this kinetic energy is the sum of two contributions,  $\epsilon = \epsilon_s + \epsilon_d$ , where  $\epsilon_s$  is the solenoidal dissipation associated with the incompressible part of the velocity field. The distribution of this dissipation is given by the standard transport equation. The dilatation dissipation  $\epsilon_d$  resulting from dilatation effects of the velocity field is given by the following expression proposed by Zeman<sup>29</sup>:  $\epsilon = \epsilon_s + \epsilon_d = \epsilon_s [1 + c_d f(M_t)]$  with  $M_t = \sqrt{(2k)/c}$ ,  $c_d = 0.75$ , and

$$\begin{cases} f(M_t) = 1 - \exp \left[ - \left( \frac{M_t - 0.1}{0.6} \right)^2 \right] & \text{if } M_t > 0.1 \\ f(M_t) = 0 & \text{if } M_t \leq 0.1 \end{cases}$$

The transport equations for  $k$  and  $\epsilon$  take the following form:

$$\begin{aligned} \frac{\partial \bar{\rho} k}{\partial t} + \bar{u}_j \frac{\partial \bar{\rho} k}{\partial x_j} &= \frac{\partial}{\partial x_j} \left[ \left( \mu + \frac{\mu_t}{\sigma_k} \right) \frac{\partial k}{\partial x_j} \right] + \mathbf{P} + \mathbf{G} - \bar{\rho} \epsilon \\ \frac{\partial \bar{\rho} \epsilon_s}{\partial t} + \bar{u}_j \frac{\partial \bar{\rho} \epsilon_s}{\partial x_j} &= \frac{\partial}{\partial x_j} \left[ \left( \mu + \frac{\mu_t}{\sigma_\epsilon} \right) \frac{\partial \epsilon_s}{\partial x_j} \right] \\ &+ \frac{\epsilon_s}{k} [C_{\epsilon 1} (\mathbf{P} + \mathbf{G}) - C_{\epsilon 2} \bar{\rho} \epsilon_s] \end{aligned}$$

Using the eddy viscosity concept, which relates the Reynolds stresses to the mean flow gradients, the production term  $\mathbf{P}$  can be written as

$$\mathbf{P} = - \overline{\rho u_i'' u_j''} \frac{\partial \bar{u}_i}{\partial x_j} = \left[ \mu_t \left( \frac{\partial \bar{u}_i}{\partial x_j} + \frac{\partial \bar{u}_j}{\partial x_i} - \frac{2}{3} \frac{\partial \bar{u}_k}{\partial x_k} \delta_{ij} \right) - \frac{2}{3} \bar{\rho} k \delta_{ij} \right] \frac{\partial \bar{u}_i}{\partial x_j}$$

where  $\mu_t$  is the turbulent viscosity given by  $\mu_t = \bar{\rho} C_\mu k^2 / \epsilon_s$ . The other production term  $\mathbf{G}$  is calculated by Jones<sup>37</sup> as

$$\mathbf{G} = \overline{u_i''} \frac{\partial \bar{p}}{\partial x_i} = \frac{\overline{\rho' u_i''}}{\bar{\rho}} \frac{\partial \bar{p}}{\partial x_i} = - \frac{1}{\bar{\rho}} \frac{\mu_t}{\sigma_t} \frac{\partial \bar{p}}{\partial x_i} \frac{\partial \bar{p}}{\partial x_i} \quad \text{with } 0.7 \leq \sigma_t \leq 1$$

Standard values of the empirical constants of the  $k-\epsilon$  model given by Launder and Spalding<sup>38</sup> are used in the calculations  $C_\mu = 0.09$ ,  $C_{\epsilon 1} = 1.44$ ,  $C_{\epsilon 2} = 1.92$ ,  $\sigma_k = 1.0$ , and  $\sigma_\epsilon = 1.3$ .

These equations are solved by the ESTET code developed by the Laboratoire National Hydraulique of the Direction des Etudes et Recherches d'Electricité de France. The algorithm is based on the projection method, introduced by Chorin<sup>39</sup> and Temam,<sup>40</sup> for the time discretization of the Navier-Stokes equations. A characteristic method is used for the convection step. The diffusion step and the pressure-continuity step, or projection step, are solved using implicit methods. The mesh is structured but irregular. Because the mean flow is axisymmetric, the calculation is carried out in a single plane. The grid size is  $200 \times 124$  points for a computational domain extending over  $20D \times 14D$ .

### Acknowledgments

This research was supported by Électricité de France and the Centre National des Études Spatiales. Computing time was provided by the Institut du Développement et des Ressources en Informatique Scientifique.

### References

- Colonus, T., Lele, S. K., and Moin, P., "The Scattering of Sound Waves by a Vortex: Numerical Simulations and Analytical Solutions," *Journal of Fluid Mechanics*, Vol. 260, Feb. 1994, pp. 271–298.
- Mitchell, B. E., Lele, S. K., and Moin, P., "Direct Computation of the Sound from a Compressible Co-Rotating Vortex Pair," *Journal of Fluid Mechanics*, Vol. 285, Feb. 1995, pp. 181–202.
- Colonus, T., Moin, P., and Lele, S. K., "Direct Computation of Aerodynamic Sound," Dept. of Mechanical Engineering, Stanford Univ., TF-65, Stanford, CA, June 1995.
- Béchara, W., Bailly, C., Lafon, P., and Candel, S., "Stochastic Approach to Noise Modeling for Free Turbulent Flows," *AIAA Journal*, Vol. 32, No. 3, 1994, pp. 455–463.
- Bailly, C., Lafon, P., and Candel, S., "A Stochastic Approach to Compute Noise Generation and Radiation of Free Turbulent Flows," AIAA Paper 95-092, June 1995.
- Bailly, C., Lafon, P., and Candel, S., "Computation of Noise Generation and Propagation for Free and Confined Turbulent Flows," AIAA Paper 96-1732, May 1996.
- Witkowska, A., Brasseur, J. G., and Juvé, D., "Numerical Study of Noise from Stationary Isotropic Turbulence," AIAA Paper 95-037, June 1995.
- Bastin, F., Lafon, P., and Candel, S., "Computation of Jet Mixing Noise from Unsteady Coherent Structures," AIAA Paper 95-039, June 1995.
- Ribner, H. S., "Quadrupole Correlations Governing the Pattern of Jet Noise," *Journal of Fluid Mechanics*, Vol. 38, No. 1, 1969, pp. 1–24.
- Hecht, A. M., Teske, M. E., and Bilanin, A. J., "Prediction Aerodynamic Sound Utilizing a Two-Point, Two-Time Turbulence Theory," AIAA Paper 81-2023, Oct. 1981.
- Béchara, W., Lafon, P., Bailly, C., and Candel, S., "Application of a  $k-\epsilon$  Model to the Prediction of Noise for Simple and Coaxial Free Jets," *Journal of the Acoustical Society of America*, Vol. 97, No. 6, 1995, pp. 3518–3531.

- <sup>12</sup>Bailly, C., Béchara, W., Lafon, P., and Candel, S., "Jet Noise Predictions Using a  $k-\epsilon$  Turbulence Model," AIAA Paper 93-4412, Oct. 1993.
- <sup>13</sup>Bailly, C., Lafon, P., and Candel, S., "Computation of Subsonic and Supersonic Jet Mixing Noise Using a Modified  $k-\epsilon$  Model for Compressible Free Shear Flows," *Acta Acustica*, Vol. 2, No. 2, 1994, pp. 110-112.
- <sup>14</sup>Goldstein, M. E., and Howes, W. L., "New Aspects of Subsonic Aerodynamic Noise Theory," NASA TN D-7158, Feb. 1973.
- <sup>15</sup>Goldstein, M. E., *Aeracoustics*, McGraw-Hill, New York, 1976, p. 278.
- <sup>16</sup>Bailly, C., Lafon, P., and Candel, S., "Prediction of Supersonic Jet Noise from a Statistical Acoustic Model and a Compressible Turbulence Closure," *Journal of Sound and Vibration*, Vol. 194, No. 2, 1996, pp. 219-242.
- <sup>17</sup>Ffowcs Williams, J. E., and Maidanik, G., "The Mach Wave Field Radiated by Supersonic Turbulent Shear Flows," *Journal of Fluid Mechanics*, Vol. 21, No. 4, 1965, pp. 641-657.
- <sup>18</sup>Khavaran, A., Krejsa, E. A., and Kim, C. M., "Computation of Supersonic Jet Mixing Noise from an Axisymmetric CD Nozzle Using a  $k-\epsilon$  Turbulence Model," AIAA Paper 92-0500, Jan. 1992.
- <sup>19</sup>Khavaran, A., Krejsa, E. A., and Kim, C. M., "Computation of Supersonic Jet Mixing Noise for an Axisymmetric Convergent-Divergent Nozzle," *Journal of Aircraft*, Vol. 31, No. 3, 1994, pp. 603-609.
- <sup>20</sup>Lighthill, M. J., "On Sound Generated Aerodynamically, I. General Theory," *Proceedings of the Royal Society of London, Series A: Mathematical and Physical Sciences*, Vol. 211, No. 1107, 1952, pp. 564-587.
- <sup>21</sup>Ffowcs Williams, J. E., "Noise Source Mechanisms," *Modern Methods in Analytical Acoustics, Lecture Notes*, Springer-Verlag, London, 1992, pp. 313-354.
- <sup>22</sup>Lilley, G. M., "On the Noise from Air Jets," Aeronautical Research Council, ARC 20-276, London, 1958.
- <sup>23</sup>Batchelor, G. K., *The Theory of Homogeneous Turbulence*, Cambridge Univ. Press, Cambridge, England, UK, 1953, Chap. 8, p. 179.
- <sup>24</sup>Bailly, C., "A Statistical Description of Supersonic Jet Mixing Noise," AIAA Paper 97-1575, May 1997.
- <sup>25</sup>Davies, P. O. A. L., Fisher, M. J., and Barratt, M. J., "The Characteristics of the Turbulence in the Mixing Region of a Round Jet," *Journal of Fluid Mechanics*, Vol. 15, No. 3, 1963, pp. 337-367.
- <sup>26</sup>Goldstein, M. E., and Rosenbaum, B., "Effect of Anisotropic Turbulence on Aerodynamic Noise," *Journal of the Acoustical Society of America*, Vol. 54, No. 3, 1973, pp. 630-645.
- <sup>27</sup>Lilley, G. M., "The Generation and Radiation of Supersonic Jet Noise, Vol. 4. Theory of Turbulence Generated Jet Noise, Noise Radiation from Upstream Sources, and Combustion Noise. Pt. 2: Generation of Sound in a Mixing Region," U. S. Air Force Aero Propulsion Lab., AFAPL-TR-72-53, Wright-Patterson AFB, OH, 1972.
- <sup>28</sup>Parthasarathy, S. P., and Massier, P. J., "Mach Wave Emission from Supersonic Jets," *AIAA Journal*, Vol. 15, No. 10, 1977, pp. 1462-1468.
- <sup>29</sup>Zeman, O., "Dilatation-Dissipation: The Concept and Application in Modeling Compressible Mixing Layers," *Physics of Fluids A*, Vol. 2, No. 2, 1990, pp. 178-188.
- <sup>30</sup>Lush, P. A., "Measurements of Subsonic Jet Noise and Comparison with Theory," *Journal of Fluid Mechanics*, Vol. 46, No. 3, 1971, pp. 477-500.
- <sup>31</sup>Tanna, H. K., Dean, P. D., and Burrin, R. H., "The Generation and Radiation of Supersonic Jet Noise. Vol. III. Turbulent Mixing Noise Data," Air Force Aero-Propulsion Lab., Lockheed-Georgia Co., AFAPL-TR-76-65, Marietta, GA, 1976.
- <sup>32</sup>Tanna, H. K., "An Experimental Study of Jet Noise, Pt. 1: Turbulent Mixing Noise," *Journal of Sound and Vibration*, Vol. 50, No. 3, 1977, pp. 405-428.
- <sup>33</sup>Seiner, J., Ponton, M. K., Jansen, B. J., and Lagen, N. T., "The Effects of Temperature on Supersonic Jet Noise Emission," AIAA Paper 92-02-046, May 1992.
- <sup>34</sup>Seiner, J. M., McLaughlin, D. K., and Liu, C. H., "Experiments on Supersonic Jet Noise," NASA TP 2072, 1982.
- <sup>35</sup>"Gas Turbine Exhaust Noise Prediction," Society of Automotive Engineers, ARP 876C, Warrendale, PA, 1985.
- <sup>36</sup>Tam, C. K. W., and Chen, P., "Turbulent Mixing Noise from Supersonic Jets," AIAA Paper 93-4408, Oct. 1993.
- <sup>37</sup>Jones, W. P., "Prediction Methods for Turbulent Flows," Von Kármán Inst. for Fluid Dynamics, Lecture Series No. 1979-2, Rhode-Saint-Genèse, Belgium, 1979.
- <sup>38</sup>Launder, B. E., and Spalding, D. B., "The Numerical Computation of Turbulent Flows," *Computer Methods in Applied Mechanics and Engineering*, Vol. 3, No. 2, 1974, pp. 269-289.
- <sup>39</sup>Chorin, A. J., "A Numerical Method for Solving Incompressible Viscous Flow Problems," *Journal of Computational Physics*, Vol. 2, 1967, pp. 12-26.
- <sup>40</sup>Temam, R., "On an Approximate Solution of the Navier-Stokes Equations by the Method of Fractional Steps: Pt. 1," *Archive for Rational Mechanics and Analysis*, Vol. 32, No. 2, 1969, pp. 135-153.

S. Glegg  
Associate Editor